Suppression of Current Quantization Effects for Precise Current Control of SPMSM using Dithering Techniques and Kalman Filter

***Abstract*—In a current-controlled PMSM drive system, accurate current measurement is extremely required for precise current control. However, current quantization error caused by Analog-to-Digital Converters is inevitable in digital control. This may induce torque ripple to deteriorate the control performance. In this paper, the combination of dithering techniques and Kalman filter is proposed to suppress the current quantization effects. Firstly, two dithered systems, namely, the subtractively dithered system and nonsubtractively dithered system, are designed to whiten the quantization error. In order to white the quantization error as well as to minimize the total noise level, the probability distribution characteristics of the metering noise is taken into account in nonsubtractively dithered system. Then, Kalman filter is designed to estimate the real current signals from the dithered current measurements. Since the variance of the total measurement error is theoretically calculable, Kalman filter can be designed analytically. The effectiveness of the proposed approach is verified through simulations and experiments using a real positioning system.**

***Index Terms*—Current control, quantization, dithering techniques, Kalman filter, motion control.**

I. Introduction

PRECISE current-controlled PMSM drive systems require accurate current measurement to produce high static and dynamic performance [1], [2]. Since the current measurement errors are caused by current sensors and Analog-to-Digital Converters (ADCs), the real current signals are not guaranteed to follow the desired references exactly. This would induce torque ripple, thus deteriorate the control performance especially when motor works at low load [3], [4]. Therefore, understanding and suppressing the effects caused by the current measurement errors have attracted a great deal of attention [5], [6].

Fig. 1 shows the typical path of current measurement. Current signals, measured by current sensors, are transformed into digital signals via ADCs after the amplitude amplification and noise filtering. During the procedures, quantization error and metering noise containing scaling error, offset error and thermal noise are introduced into the control system. We assume that the measurement system is well tuned so that the scaling error and the offset error considered in [4], [5] can be ignored. In this case, the metering noise mainly caused by the thermal drift of the analog devices is regarded as white noise. On the other hand, the quantization error arises between the input and the output of an ADC because the analog current signal may assume any value within the input range of the ADC while the output data are finite precision samples [7].

Quantization error behaves as highly colored noise and cannot be ignored in many cases. It is reported that current quantization error would affect the accuracy of the rotor position estimation when high frequency signal injection method is used for motor sensorless control [8]–[10]. In order to suppress the quantization effects, high-resolution ADCs are commonly exploited to reduce the quantization level. However, it may not only increase the implementation cost, but also decrease the sample rate of ADCs [7]. In order to cope with the quantization effects, some model-based methods are proposed to estimate the real values from the quantized outputs [11], [12]. However, the assumption that the quantization error is white noise may not be satisfied in real situations where the quantization level is relatively high.

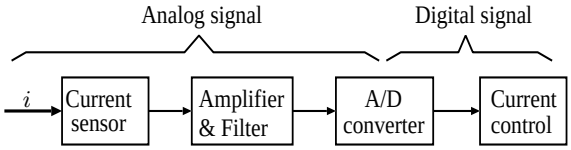

Fig. 1. Path of current measurement.

It is known that white noise is much easier to be reduced than other colored noise for it contains equal power at any center frequency. Many approaches, such as Linear-Quadratic-Gaussian (LQG) controller design method, are very effective and robust if the noise introduced into the system is white [13]. Motivated by this perspective, dithering techniques had been proposed to whiten the quantization error in the literature [14], [15], [17], [18]. However, the additional noise may increase the wide-band noise level to reduce signal-to-noise ratio, which may result in no additional improvement. In order to overcome the drawback, dithering techniques combined with Kalman filter is proposed in [16]. We extend the range of application of the approach in this study. Firstly, dither design of nonsubtractively dithered system for two common cases that the metering noise is uniform and the metering noise is Gaussian are proposed. Secondly, an exhaustive evaluation of quantization effects and the dithering techniques in d, q-axis currents is included. Finally, the proposed approaches are implemented to a real positioning system to verify their effectiveness.

The remainder of this paper is organized as follows. Section II introduces the model of plant. The dithering techniques and Kalman filter for suppressing quantization effects are presented in Section III. Sections IV and V demonstrate the effectiveness of the proposed approach by simulations and experiments. Finally, the conclusion is given in Section VI.

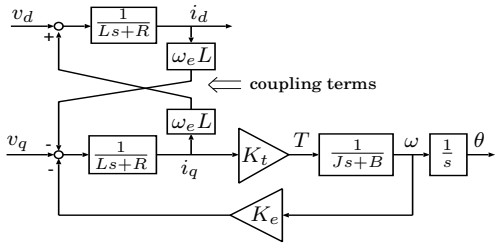

Fig. 2. Model of surface Permanent Magnet synchronous motor.

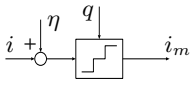

Fig. 3. Model of the current measurement. η is the metering noise, and q is the quantization error.

II. System description

Current control for a Surface Permanent Magnet Synchronous Motor (SPMSM) is considered. According to Park transform, d, q-axis voltage equations are expressed by [4]

$$\begin{bmatrix} v_d \\ v_q \end{bmatrix} = \begin{bmatrix} Ls+R & -\omega_e L \\ \omega_e L & Ls+R \end{bmatrix} \begin{bmatrix} i_d \\ i_q \end{bmatrix} + \omega K_e \begin{bmatrix} 0 \\ 1 \end{bmatrix}, \quad (1)$$

where s denotes the Laplace operator, $i_{d,q}$ denote the d, q-axis currents, $v_{d,q}$ denote the d, q-axis voltages, L is the stator inductance, R is the stator resistance, K_e is the back-EMF constant, and ω_e and ω are the field angular speed and the motor speed, respectively. The model is shown in Fig. 2. Define v'_d and v'_q by

$$v'_d := v_d + \omega_e L i_q, \quad (2)$$

$$v'_q := v_q - (\omega_e L i_d + \omega K_e), \quad (3)$$

the equation (1) can be rewritten as

$$\begin{bmatrix} v'_d \\ v'_q \end{bmatrix} = \begin{bmatrix} Ls+R & 0 \\ 0 & Ls+R \end{bmatrix} \begin{bmatrix} i_d \\ i_q \end{bmatrix}. \quad (4)$$

According to Park Transform, the following equation is obtained:

$$\begin{bmatrix} i_u \\ i_v \\ i_w \end{bmatrix} = \frac{2}{3} \frac{1}{Ls+R} \begin{bmatrix} 1 & -\frac{1}{2} & -\frac{1}{2} \\ -\frac{1}{2} & 1 & -\frac{1}{2} \\ -\frac{1}{2} & -\frac{1}{2} & 1 \end{bmatrix} \begin{bmatrix} v'_u \\ v'_v \\ v'_w \end{bmatrix}, \quad (5)$$

where $[v'_u\ v'_v\ v'_w]^T$ is the fictive voltage vector calculated from $[v'_d\ v'_q]^T$.

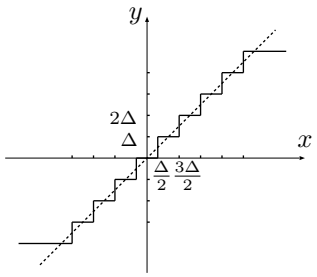

Fig. 4. Quantization characteristic. Δ is the quantization step.

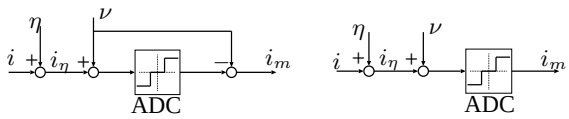

Fig. 5. Dithering method for current quantization. (a) Subtractively dithered method; (b) Nonsubtractively dithered method.

In digital control, current signals are measured by current sensors and quantized by ADCs before they are used for feedback. During the procedures, metering noise η and quantization error q are introduced into the control system, as shown in Fig. 3. An ideal ADC is a nonlinear device having a staircase-type I/O relation, as shown in Fig. 4. Assuming that the input is always within the measurement range of ADCs, the output y can be expressed in terms of the input x as

$$y = Q(x) = \Delta \left\lfloor \frac{x}{\Delta} + \frac{1}{2} \right\rfloor, \quad (6)$$

where $Q(\cdot)$ is the quantization operator, $\lfloor \cdot \rfloor$ is the floor operator, and Δ is the quantization step defined by

$$\Delta = \frac{I_0}{2^{N_b - 1}}. \quad (7)$$

Here, I_0 is the one-sided measurement range of current sensor and N_b is the resolution of the ADC. The quantization error is defined by

$$q := Q(x) - x. \quad (8)$$

q is dependent of x unless x satisfies the so-called band-limited condition [21], which is not always the case.

III. Dithering techniques and Kalman filter for current quantization

A. Subtractively dithered system

Subtractively dithered system for suppressing current quantization error is shown in Fig. 5(a). ν is the dither signal. The measurement error can be expressed by

$$\begin{aligned} e_i &= i_m - i \\ &= Q(i_\eta + \nu) - (i_\eta + \nu) + \eta \\ &= q(i_\eta + \nu) + \eta. \end{aligned} \quad (9)$$

According to *Schuchman's Condition* [18], $q(i_\eta + \nu)$ is independent of i_η if ν is uniform in $[-\frac{\Delta}{2}\ \frac{\Delta}{2}]$. Suppose η is white noise, the mean and variance of e_i are calculated by [16]

$$E[e_i] = 0, \quad (10)$$

$$E[e_i^2] = E[\eta^2] + \frac{\Delta^2}{12}, \quad (11)$$

where $E[u]$ means the expectation of u.

B. Nonsubtractively dithered system

Nonsubtractively dithered system for suppressing current quantization is shown in Fig. 5(b). The current measurement error is expressed by

$$\begin{aligned} e_i &= i_m - i \\ &= Q(i_\eta + \nu) - i_\eta + \eta \\ &= q(i_\eta + \nu) + \nu + \eta, \end{aligned} \tag{12}$$

According to the *Theorem* in [19], we can obtained that the dither with the triangular-pdf

$$p_\nu(\epsilon) = \begin{cases} \frac{1}{\Delta^2}(\epsilon + \Delta), & -\Delta < \epsilon \le 0 \\ \frac{1}{\Delta^2}(-\epsilon + \Delta), & 0 < \epsilon \le \Delta \\ 0, & \text{otherwise}, \end{cases} \tag{13}$$

is the unique choice to render the mean and the variance of $q(i_\eta + \nu) + \nu$ be independent of the input i_η. ν and e_i have the following mean and variance:

$$E[\nu] = 0, \tag{14}$$

$$E[\nu^2] = \frac{\Delta^2}{6}, \tag{15}$$

$$E[e_i] = 0, \tag{16}$$

$$E[e_i^2] = E[\eta^2] + \frac{\Delta^2}{4}. \tag{17}$$

$E[e_i^2]$ may be too large to be acceptable. In the following, the probability distribution characteristics of η is utilized to reduce $E[e_i^2]$.

For convenience, we denote w as the sum of the dither ν and the metering noise η:

$$w := \eta + \nu. \tag{18}$$

According to (12), the measurement error e_i is expressed by

$$e_i = q(i + w) + w. \tag{19}$$

In order to render e_i be independent of i, w is required to be the triangular noise (13) [19]. According to Convolution Theorem and inverse Fourier Transform, a theoretical selection of ν is that p_ν should satisfy

$$p_\nu = \boldsymbol{\mathcal{F}}^{-1} \frac{\text{sinc}^2(\pi\Delta u)}{P_\eta(u)} du. \tag{20}$$

Here, $\text{sinc}^2(\pi\Delta u)$ and $P_\eta(u)$ are the characteristic functions of the triangular-pdf noise (13) and η, respectively.In this way, the variance of e_i is calculated by

$$E[e_i^2] = \frac{\Delta^2}{4}. \tag{21}$$

This implies that the variance of e_i is not affected by η and smaller than (17).

Usually, the dither ν with the pdf calculated by (20) is very hard to be generated in practical situations. In the following, two common cases that η is uniform noise and η is Gaussian noise are discussed.

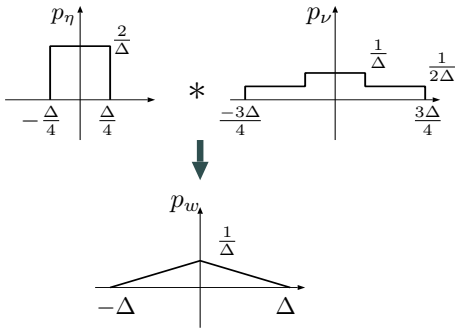

Fig. 6. Example of **Proposition 1** in the case of $N = 2$. '$*$' means the operator of convolution.

1) The metering noise is uniform noise: In this case, the following result is achieved:

Proposition 1: Suppose that η is uniform noise with the probability density function

$$p_\eta(\epsilon) = \begin{cases} \frac{N}{\Delta}, & -\frac{\Delta}{2N} < \epsilon \le \frac{\Delta}{2N} \\ 0, & \text{otherwise}, \end{cases} \tag{22}$$

where $N \in \mathcal{N}$, then the probability density function of w is the triangular-pdf (13) if the probability density function of ν satisfies

$$p_\nu(\epsilon) = \begin{cases} \frac{1}{N\Delta}, & \begin{cases} -\frac{2N-1}{2N}\Delta < \epsilon \le -\frac{2N-3}{2N}\Delta \\ \frac{2N-3}{2N}\Delta < \epsilon \le \frac{2N-1}{2N}\Delta \end{cases} \\ \frac{2}{N\Delta}, & \begin{cases} -\frac{2N-3}{2N}\Delta < \epsilon \le -\frac{2N-5}{2N}\Delta \\ \frac{2N-5}{2N}\Delta < \epsilon \le \frac{2N-3}{2N}\Delta \end{cases} \\ \vdots & \vdots \\ \frac{i}{N\Delta}, & \begin{cases} -\frac{2(N-i)+1}{2N}\Delta < \epsilon \le -\frac{2(N-i)-1}{2N}\Delta \\ \frac{2(N-i)-1}{2N}\Delta < \epsilon \le \frac{2(N-i)+1}{2N}\Delta \end{cases} \\ \vdots & \vdots \\ \frac{N-1}{N\Delta}, & \begin{cases} -\frac{3}{2N}\Delta < \epsilon \le -\frac{1}{2N}\Delta \\ \frac{1}{2N}\Delta < \epsilon \le \frac{3}{2N}\Delta \end{cases} \\ \frac{1}{\Delta}, & -\frac{1}{2N}\Delta < \epsilon \le \frac{1}{2N}\Delta \\ 0, & \text{otherwise}, \end{cases} \tag{23}$$

where $i = 1, 2, \cdots, N-1$.

□

Proposition 1 can be proved according to the Convolution Theorem. Fig. 6 illustrates the convolution of p_η and p_ν in the case of $N = 2$.

In the case that the condition (22) is not satisfied, say, η is uniform in $\left[-\frac{\Delta}{2(K+\alpha)} \quad \frac{\Delta}{2(K+\alpha)}\right]$ for some $K \in \mathcal{N}$ and $-0.5 < \alpha \le 0.5$, the principle of proximity can be applied for p_η.

2) Metering error is Gaussian noise: In this case, the optimal design of ν by (20) is unavailable. Therefore, a suboptimal design of ν is taken into account. The following proposition is achieved:

Proposition 2: Suppose that the metering error η is Gaussian noise and has the Normal distribution

$$p_\eta(\epsilon) = \frac{1}{\sqrt{2\pi\sigma^2}} \exp\left\{-\frac{1}{2}\frac{\epsilon^2}{\sigma^2}\right\}, \quad 0 < \sigma^2 < \frac{\Delta^2}{6}, \tag{24}$$

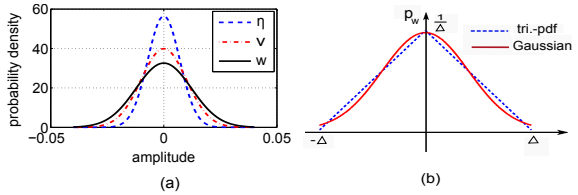

Fig. 7. (a): Illustration of $w = \eta + \nu$ from the view of probability distribution when η and ν are Gaussian. (b): Comparison of triangular-pdf and Gaussian distribution.

where σ is the standard deviation. Then, w is Gaussian and has the same variance with the triangular dither (13) if p_ν satisfies

$$p_\nu(\epsilon) = \frac{1}{\sqrt{2\pi(\frac{\Delta^2}{6} - \sigma^2)}} \exp\left\{-\frac{1}{2}\frac{\epsilon^2}{\frac{\Delta^2}{6} - \sigma^2}\right\}. \tag{25}$$

□

Proposition 2 can be proved according to Convolution Theorem. In the case of $\sigma^2 \geq \frac{\Delta^2}{6}$, η can be regarded to be large enough to whiten the quantization error so that ν becomes unnecessary. Fig. 7(a) illustrates the sum of two variables from the view of probability distribution.

The comparison between the Normal distribution and the triangular distribution with the same variance is shown in Fig. 7(b). For practical implementation, a dither with Normal distribution has almost the same advantage to whiten the quantization error. A further insight into the discussion is provided in [20].

C. Kalman filter for noise suppression

A state-space realization of the model (5) is expressed as

$$\dot{\boldsymbol{x}} = \boldsymbol{A}\boldsymbol{x} + \boldsymbol{B}\boldsymbol{u}, \tag{26}$$

$$\boldsymbol{y} = \boldsymbol{C}\boldsymbol{x}, \tag{27}$$

where $\boldsymbol{x} = [i_u \ i_v \ i_w]^T$, $\boldsymbol{u} = [v'_u \ v'_v \ v'_w]^T$ and

$$\boldsymbol{A} = \mathrm{diag}\left(-\frac{R}{L}, -\frac{R}{L}, -\frac{R}{L}\right),$$

$$\boldsymbol{B} = \frac{2}{3L}\begin{bmatrix} 1 & -\frac{1}{2} & -\frac{1}{2} \\ -\frac{1}{2} & 1 & -\frac{1}{2} \\ -\frac{1}{2} & -\frac{1}{2} & 1 \end{bmatrix},$$

$$\boldsymbol{C} = \boldsymbol{I}_3,$$

where $\boldsymbol{I}_n$ denotes the identity matrix with size n. Based on this model, Kalman filter is formulated by

$$\dot{\hat{\boldsymbol{x}}} = \boldsymbol{A}\hat{\boldsymbol{x}} + \boldsymbol{B}\boldsymbol{u} + \boldsymbol{L}_k(\boldsymbol{y} - \boldsymbol{C}\hat{\boldsymbol{x}}), \tag{28}$$

where $\hat{\boldsymbol{x}}$ is the estimation of $\boldsymbol{x}$, and $\boldsymbol{L}_k$ is Kalman gain calculated via $\boldsymbol{L}_k = \boldsymbol{P}\boldsymbol{C}^T\boldsymbol{R}_c^{-1}$. Here, $\boldsymbol{R}_c$ is the covariance of measurement noise and $\boldsymbol{P}$ is the solution of Riccati equation

$$\boldsymbol{A}\boldsymbol{P} + \boldsymbol{P}\boldsymbol{A}^T - \boldsymbol{P}\boldsymbol{C}^T\boldsymbol{R}_c^{-1}\boldsymbol{C}\boldsymbol{P} + \boldsymbol{Q}_c = \boldsymbol{0}, \tag{29}$$

where $\boldsymbol{Q}_c$ is the covariance of the input disturbances. When dithering techniques proposed in subsections III-A and III-B are applied, the variance of the e_i can be exactly calculated so that $\boldsymbol{R}_c$ can be analytically determined.

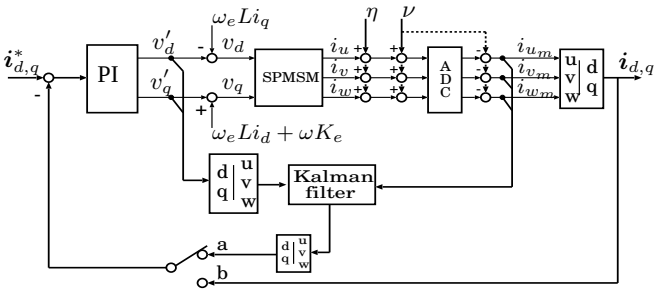

Fig. 8. Block diagram of current control for simulations.

TABLE I
PARAMETERS OF SPMSM FOR SIMULATION

Inductance L	7.2	mH
Resistance R	2.16	Ω
Inertia J	0.001	kg·m^2
Viscosity B	0.01	N·m/(rad/s)
Thrust coefficient K_t	0.715	N·m/A
Bach-EMF constant K_e	74.9	mV/(rad/s)

IV. SIMULATIONS

The simulations are performed to verify the effectiveness of the dithering techniques and Kalman filter. The control block diagram is shown in Fig. 8. The parameters of SPMSM used for simulation are shown in Table I. Decoupling control method and a proportional-integral compensator are applied as the current controller. For evaluation, V-phase and d, q-axis current measurement errors and estimation errors are defined:

$$e_{iv} := i_{v_m} - i_v, \tag{30}$$

$$e_{id} := i_{d_m} - i_d, \tag{31}$$

$$e_{iq} := i_{q_m} - i_q, \tag{32}$$

$$\hat{e}_{iv} := \hat{i}_v - i_v, \tag{33}$$

$$\hat{e}_{id} := \hat{i}_d - i_d, \tag{34}$$

$$\hat{e}_{iq} := \hat{i}_q - i_q, \tag{35}$$

where, i_{v_m} and $\hat{i}_v$ are the measured V-phase current values and the estimated current values, respectively. Since U,W-phase currents have the same results with V-phase current, we omit the discussion of U,W-phase currents. i_{d,q_m} and $\hat{i}_{d,q}$ are the d, q-axis currents calculated from the the measured currents and the estimated currents by Park Transform, respectively.

In the setup, ADCs with a resolution of 10-bit and current sensors whose measurement range is ± 50 A are supposed to be used. The resulting quantization step is $\Delta = 50/2^9$. The metering noise η is set to be uniform in $[-\frac{\Delta}{4}\ \frac{\Delta}{4}]$. The reference current signal is set as $i_q^* = 0.5 \sin 314t$ and $i_d^* = 0$. The following five cases are examined:

- Case 1: Conventional method without dither and without Kalman filter;
- Case 2: Subtractive dither without Kalman filter;
- Case 3: Nonsubtractive dither (25) without Kalman filter;
- Case 4: Subtractive dither with Kalman filter;
- Case 5: Nonsubtractive dither (25) with Kalman filter.

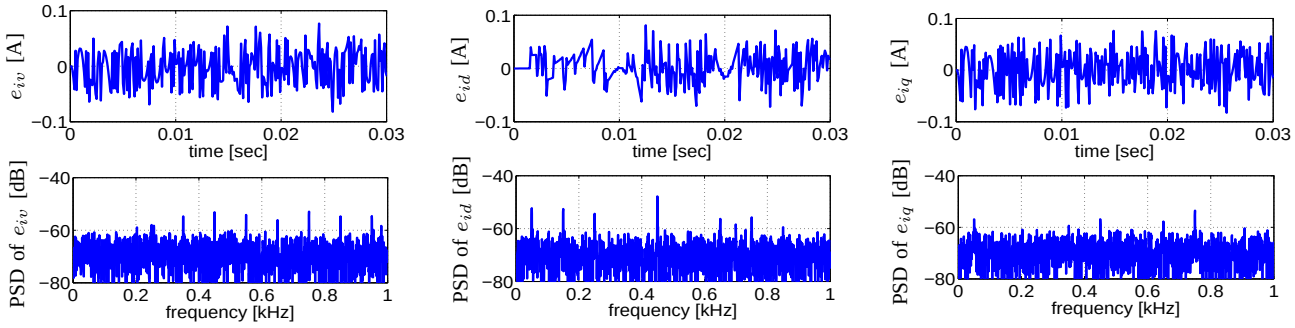

(a) Comparison of V-phase current. (b) Comparison of d-axis current. (c) Comparison of q-axis current.

Fig. 9. Simulation results of Case 1: without dither and without Kalman filter.

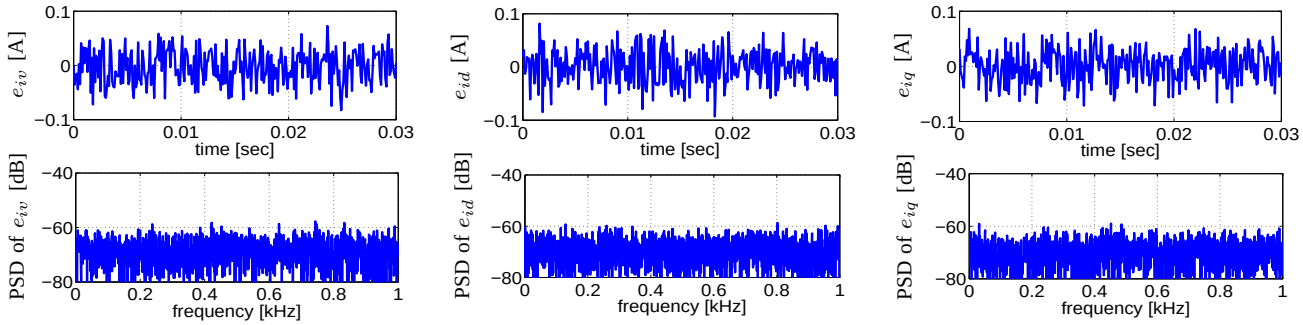

(a) Comparison of V-phase current. (b) Comparison of d-axis current. (c) Comparison of q-axis current.

Fig. 10. Simulation results of Case 2: with subtractive dither and without Kalman filter.

The simulation results are shown in Figs. 9∼13. Power spectral density (PSD) of the measurement errors is exploited to evaluate the performance of dithering techniques. In Case 1, we can see that the harmonics caused by quantization exist not only in V-phase current signal, but also in d, q-axis current signals. The harmonics are reduced when dithering techniques are applied, as shown in Fig. 10 and Fig. 11. These results indicate that current quantization errors are whitened by both the subtractively dithered method and nonsubtractively dithered method. The comparison of the measurement errors evaluated via Root-Mean-Square (RMS) and maximum value of PSD is shown in Table II. Though the average noise level is augmented by nonsubtractively dithered method, the maximum value of PSD is reduced drastically.

The results of dithering techniques combined with Kalman filter are shown in Fig. 12 and Fig. 13. It is shown that the estimated errors are far smaller than the measurement errors, which means that the designed Kalman filter can estimate the current signals exactly.

TABLE II
COMPARISON OF THE MEASUREMENT ERRORS (SIMULATION RESULTS)

situations		Case 1	Case 2	Case 3
e_{iv}	RMS value ($\times 10^{-2}$)	3.05	3.14	4.91
	PSD$_{\text{max.}}$ value [dB]	-52.89	-57.73	-55.04
e_{id}	RMS value ($\times 10^{-2}$)	3.33	3.17	4.91
	PSD$_{\text{max.}}$ value [dB]	-47.78	-58.68	-58.23
e_{iq}	RMS value ($\times 10^{-2}$)	3.11	3.14	4.93
	PSD$_{\text{max.}}$ value [dB]	-53.50	-58.97	-57.92

V. EXPERIMENTS

A. Description of the experiment system

The high precision stage is shown in Fig. 14, and its parameters are shown in Table III. The stage is a simplified model of the scanners in exposure systems used for the fabrication of integrated circuits. Two linear motors located at the both sides of the carriage are applied to drive the stage. An air guide system is introduced to reduce the friction between the stator and the slider of the motors. U, W-phase current signals are measured by FA-050PV (LEM®) whose measurement range is ± 50A. The signals are then converted into digital signals via high-precise ADCs whose resolution is 14-bit. DSP(TMS320C6713, 225MHz) is used as the processor to implement the controllers and the proposed approaches.

A two-degree-of-freedom controller is exploited for position control [22], and the resulting bandwidth of the close-loop system is 10 Hz. The block diagram of control system is shown

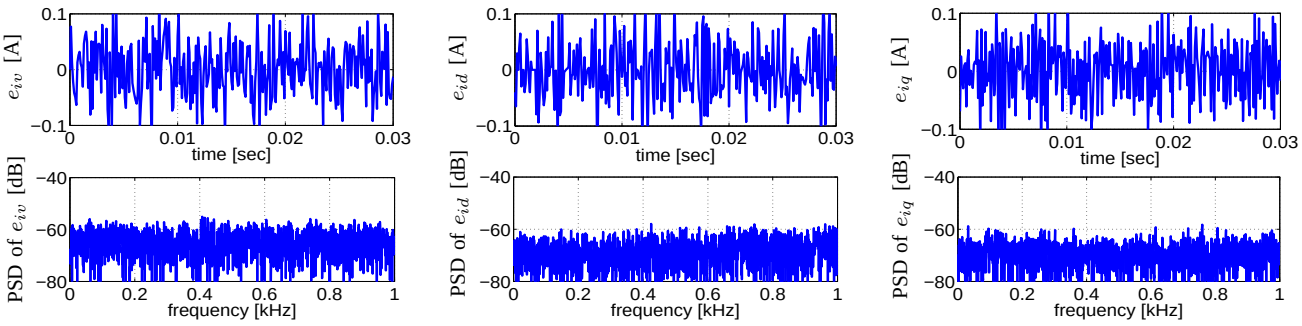

(a) Comparison of V-phase current. (b) Comparison of d-axis current. (c) Comparison of q-axis current.

Fig. 11. Simulation results of Case 3: with nonsubtractive dither and without Kalman filter.

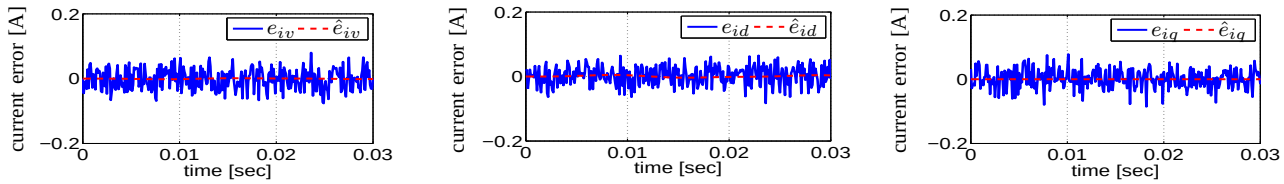

(a) Comparison of V-phase current. (b) Comparison of d-axis current. (c) Comparison of q-axis current.

Fig. 12. Simulation results of Case 4: with subtractive dither as well as Kalman filter.

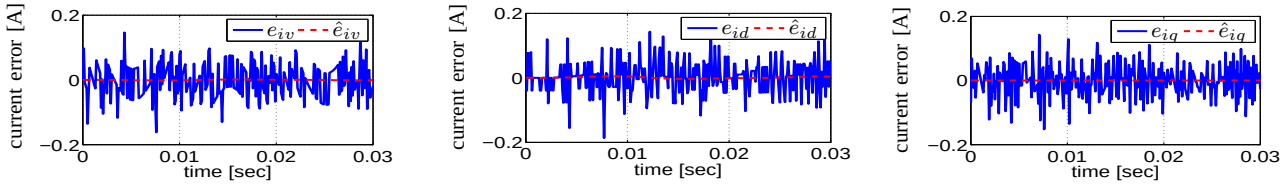

(a) Comparison of V-phase current. (b) Comparison of d-axis current. (c) Comparison of q-axis current.

Fig. 13. Simulation results of Case 5: with nonsubtractive dither as well as Kalman filter.

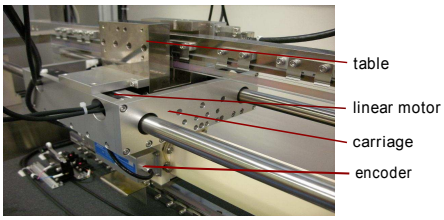

Fig. 14. Experimental device.

TABLE III
PARAMETERS OF STAGE

Inductance L	15.5	mH
Resistance R	20.5	Ω
Mass M	14.7	kg
Viscosity B	24	N/(m/s)
Thrust coefficient K_t	26.5	N/A
Bach-EMF constant K_e	16	V/(m/s)

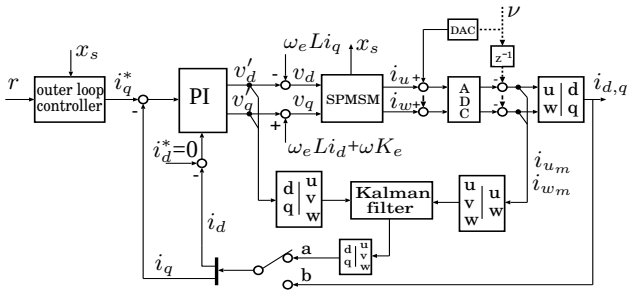

Fig. 15. Block diagram of control system.

in Fig. 15. Kalman filter is used if the switch is turned to 'a'.

In order to verify the effectiveness of the dithering techniques, the resolution of the ADCs is dropped to 10-bit by software so that the resulting current quantization step is $\Delta = 0.0977\,\mathrm{A}$. For comparison, a precise current probe

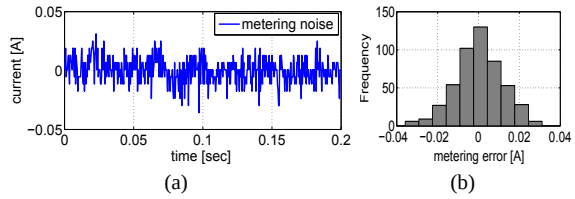

(a) (b)

Fig. 16. Example of the metering noise (a) and its histogram analysis (b).

(Tektronix®) is used to measure the real current signal. Dither signals are generated in DSP by "Box-Muller method" [23] and then converted into analog signals via D/A converters whose resolution is 16-bit.

At first, the probability distribution of the metering noise is analyzed. A current signal measured by current measurement system without executing the control system is used for analyzing the characteristics of the metering noise η. A sample of η in time domain is shown in Fig. 16(a). The corresponding histogram plot is shown in Fig. 16(b). It is observed that the metering noise can be approximated with Gaussian noise. By calculation, the variance of η is $E[\eta^2] = 1.1218 \times 10^{-4}$. Based on this value, the nonsubtractive dither is designed based on (25). The covariance matrix R_c for Kalman filter is designed based on the error variances (11) and (21). $\boldsymbol{Q}_c$ is properly set as $\boldsymbol{Q}_c = \mathrm{diag}(0.05,\ 0.05,\ 0.05)$.

B. Experimental evaluation

The trajectory reference including acceleration, uniform motion, deceleration is given, as shown in Fig. 17. Five cases defined in Section IV are used for evaluation. For comparison, the position tracking error is defined as follows:

$$e_s := r - x_s, \tag{36}$$

where r is the reference trajectory and x_s is the position of the stage.

Fig. 18 shows the results of Cases 1∼3. For simplicity, only U-phase currents are used for analysis. In Case 1, the harmonics caused by quantization appear especially at low frequencies, as shown in Fig. 18(a). On the other hand, the power spectral density of e_{iu} is flat all over the frequency domain when dithering techniques are applied, as shown in Fig. 18(b,c). These results indicate that the quantization error is whitened by the dithering techniques. The RMS of e_{iu} and the maximum value of its PSD are summarized in Table IV. The comparison of position tracking performance is shown in Fig. 19. It is also observed that the tracking performance is improved by dithering techniques.

Fig. 20 shows the results of Case 4 and Case 5. We can see that the estimation errors are much smaller than the measurement errors. These results indicate that the estimated currents are very close to real current signals. Therefore, Kalman filter can result in better control performance, as shown in Fig. 21. The comparison of position tracking performance of all five cases is summarized in Table V. It is demonstrated that the combination of dithering techniques and Kalman filter can suppress quantization effects and significantly improve the control performance.

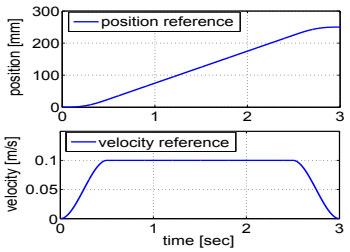

Fig. 17. Position and velocity reference.

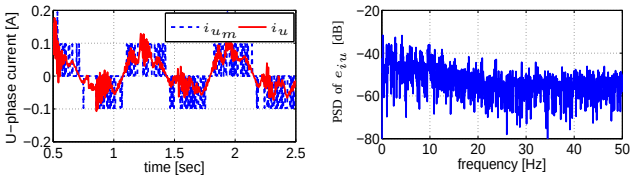

(a) Experimental results of Case 1.

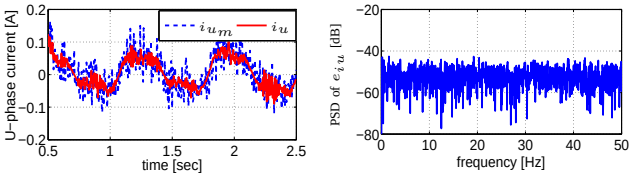

(b) Experimental results of Case 2.

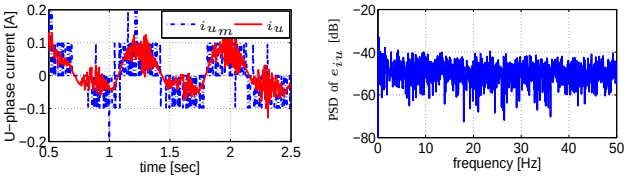

(c) Experimental results of Case 3.

Fig. 18. Experimental results without applying Kalman filter.

VI. Conclusion

In this paper, the combination of dithering techniques and Kalman filter for suppressing current quantization effects is proposed. In order to whiten the quantization error and reduce the total measurement noise level at the same time, the probability characteristics of the metering noise is utilized to design the nonsubtractively dithered system. Furthermore, Kalman filter is applied to estimate the real current signals from the dithered measurement signals. Since the variance of the total measurement error is calculable, the covariance matrix for Kalman filter becomes explicit. The simulation and experimental results demonstrate the effectiveness of the proposed method.

References

[1] Mohamed-Wissem Naouar, E. Monmasson, A. A. Naassani, I. S. BElkhodja and N. Patin, "FPGA-Based Current Controllers

TABLE IV
Comparison of the measurement error (experimental results)

	case 1	case 2	case 3
RMS of e_{i_u} ($\times 10^{-3}$)	1.14	1.07	3.12
PSDmax. [dB]	−31.8	−42.3	−37.9

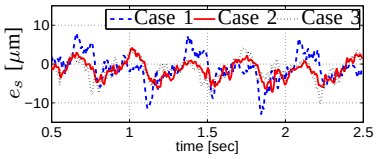

Fig. 19. Comparison of position tracking errors of Case 1∼3.

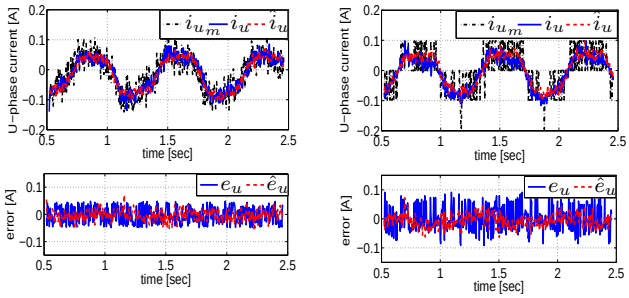

(a) (b)

Fig. 20. Experimental results when dithering techniques combined with Kalman filter is applied. (a) is the results of case 4, and (b) is the results of case 5.

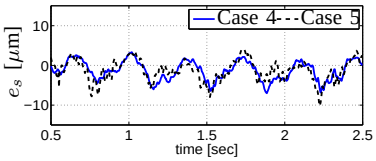

Fig. 21. Comparison of position tracking errors of Case 4 and Case 5.

TABLE V
COMPARISON OF POSITION TRACKING ERROR (EXPERIMENTAL RESULTS)

Case	1	2	3	4	5
RMS of e_s [μm]	3.81	2.83	3.01	2.78	2.79
Max. of e_s [μm]	12.90	7.23	10.21	7.03	7.81

for AC Machine Drives–A Review", *IEEE Trans. Indust. Electron.*, vol. 54, no. 4, pp. 1907–1925, Aug. 2007.

[2] Y. Cho, T. LaBella, and J.S. Lai, "A Three-Phase Current Reconstruction Strategy With Online Current Offset Compensation Using a Single Current Sensor", *IEEE Trans. Indust. Electron.*, vol. 59, no. 7, pp. 2924–2933, Jul. 2012.

[3] J. Holtz and J. Quan, "Sensorless Vector Control of Induction Motors at Very Low Speed Using a Nonlinear Inverter Model and Parameter Identification", *IEEE Trans. Indust. Appl.* , vol. 38, no. 4, pp. 1087–1095, Jul./Aug. 2002.

[4] N. Miyamoto and J, Ohishi, "Online Tuning Method for Current Measurement Offsets and Gain Deviations for SPMSM", *IECON2012 - 38th Annu. Conf. IEEE Ind. Electron. Soc.*, , Montreal, Oct., 2012, pp. 1940–1945.

[5] D. W. Chung, and S. K. Sul, "Analysis and Compensation of Current Measurement Error in Vector-Controlled AC Motor Drives", *IEEE Trans. Indust. Appl.* , vol. 34, no. 2, pp. 340–345, Mar./Apr. 1998.

[6] M. Kim, S. K. Sul, and J. Lee, "Compensation of Current Measurement Error for Current-Controlled PMSM Drives", *IEEE Energy Convers. Congr. Expo.* , Raleigh, Sep. 2012, pp. 487–494.

[7] R.H. Walden, Analog-toDigital Converter Survey and Analysis, *IEEE J. Sel. Areas Commun.*, vol. 17, no. 4, Apr. 1999.

[8] J. H. Jang, S. K. Sul, and Y. C. Son, "Current Measurement Issues in Sensorless Control Algorithm using High Frequency Signal Injection Method", *IEEE Ind. App. Soc. Annu. Meeting* , vol. 2, Salt Lake City, Oct. 2003, pp. 1134–1141.

[9] Z. Q. Zhu, and L. M. Gong, "Investigation of Effectiveness of Sensorless Operation in Carrier-Sinal-Injection-Based Sensorless-Control Methods", *IEEE Trans. Ind. Electron.*, vol. 58, no. 8, pp. 3431–3439, Aug. 2011.

[10] P. Garcia, F. Briz, M. W. Degner, and D. D. Reigosa, "Accuracy, Bandwidth, and Stability Limits of Carrier-Signal-Injection-Based Sensorless Control Method", *IEEE Trans. Ind. Appl.*, vol. 43, no. 4, pp. 990–1000, Jul./Aug. 2007.

[11] A. S. Hodel, and J. Y. Hung, "A State Estimator with Reduced Sensitivity to Sensor Quantization", *IECON'03 - 29th Annu. Conf. IEEE Ind. Electron. Soc.*, Roanoke, Nov. 2003, pp. 586–590.

[12] S. J. Kwon, W. K. Chung, and Y. Youm, "A Combined Observer for Robust State Estimation and Kalman filtering", in *Proc. Amer. Control Conf.*, **3**, Denver, Colorado, Jun. 2003, pp. 2459-2464.

[13] A. Molin, and S. Hirche, "On LQG Joint Optimal Scheduling and Control under Communication Constraints", *48th IEEE Conf. Decision Control*, Shanghai, Dec. 2009, pp. 5832–5838.

[14] S. H. Yu, "Feedback Dithering for Decorrelating Quantization Noise and Enhancing SNDR", *IEEE Trans. Control Syst. Technol.* , vol. 20, no. 3, May 2012.

[15] F. Gustafsson, and R. Karlsson, "Generating Dithering Noise for Maximum Likelihood Estimation from Quantized Data", *Automatica*, 49, pp. 554–560, 2012.

[16] H. Zhu, H. Fujimoto, "Overcoming Current Quantization Effects for Precise Current Control by Combining Dithering Techniques and Kalman filter", *IECON2012 - 38th Annu. Conf. IEEE Ind. Electron. Soc.*, Montreal, Oct. 2012, pp. 3806–3811.

[17] S. P. Lipshitz, R. A. Wannamaker, and J. Vanderkooy, "Quantization and Dither: A Theoretical Survey", *J. Audio Eng. Soc.* , vol. 40, no.5, pp. 355–375, May 1992.

[18] L. Schuchman, "Dither Signals and Their Effect on Quantization Noise", *IEEE Trans. Commun. Technol.* , pp. 162–165, Dec. 1964.

[19] R. A. Wannamaker, S. P. Lipshitz, J. Vanderkooy,and J. N. Wright, "A Theory of Nonsubtractive Dither", *IEEE Trans. Signal Process.* , vol. 48, no.2, pp. 499–516, Feb. 2000.

[20] M. F. Wagdy and M. Goff, Linearizing Average Transfer Characteristics of Ideal ADC's via Analog and Digital Dither, *IEEE Trans. Instrum. Meas.*, vol. 43, no. 2, pp. 146–150, Apr. 1994.

[21] B. Widrow, I. Kollár, and M. Liu, Statistical Theory of Quantization, *IEEE Trans. Instrum. Meas.*, vol. 45, no. 2, pp. 353–361, Apr. 1996.

[22] H. Fujimoto, Y. Hori, and A. Kawamura, "Perfect tracking control based on multirate feed forward control with generalized sampling periods," *IEEE Trans. Ind. Electron.*, vol. 48, no. 3, pp. 636–644, 2001.

[23] M. E. Muller, A Comparison of Methods for Generating Normal Deviates on Digital Computers, *J. ACM*, vol. 6, no. 3, pp. 376–383, Jul. 1959.

[24] I. Paraskevakos, and V. Paliouras, A Flexible High-Throughput Hardware Architecture for A Gaussian Noise Generator, *IEEE Int. Conf. Acoust., Speech, Signal Process.*, Prague, Czech, May 2011, pp. 1673–1676.